Journal of Medical Engineering & Technology, Vol.41 Iss 1 pp. 72 – 80 (Final manuscript)

A Study of Nano-biosensors and their Output Amplitude Analysis Algorithms

Teh Yi Jun[1], Asral Bahari Jambek[2] and Uda Hashim[3]
[1,2]*School of Microelectronic Engineering, Universiti Malaysia Perlis, Perlis, Malaysia*
[3]*Insituite of Nano Electronic Engineering, Universiti Malaysia Perlis, Perlis, Malaysia*
Email: [1]kelvinteh90@gmail.com, [2]asral@unimap.edu.my, [3]uda@unimap.edu.my

***Abstract*— The aim of this paper is to discuss the latest nano-biosensor technologies and existing signal analyser algorithm methods so that an automatic and portable nano-biosensor analyser can be realized. In this paper, the latest nano-biosensors are reviewed and particular attention is given to sensors that provide amplitude changes at their output. To provide an automatic signal analysis of these changes, existing signal processing algorithms for peak detection are also discussed in detail.**

***Index Terms*— Nano-bio sensor; Bio sensor signal analysis.**

1. INTRODUCTION

Over the past decade, nano technologies have grown rapidly in popularity. Advantage has been taken of nanoscale biosensors to improve their sensitivity due to their superior properties compared to existing sensors. Nanoscale biosensors are able to perform detection on smaller sample compared to normal biosensors. This reduce the sample requires during laboratory experiment. Nanoscale biosensors can also perform detection on sample that contains one or few target particles in nanoscale. Therefore, this given advantages to perform earlier disease detection. However, to perform earlier disease detection, signal analysis of the nanoscale biosensor output is required.

The nano-biosensor signal will respond in terms of amplitude, frequency, phase and time interval. Different signal responses require different analysis algorithms to analyse the signal. Hence, an efficient signal analysis algorithm is required to support the growth of nanoscale biosensors. Existing signal analysis methods mostly are desiged for normal biosensors. The output of nanoscale biosensor is more sensitive compared to normal biosensors in term of amplitude level and noise level. Hence, higher accuracy and sensitivity signal analysis method is required.

In conventional methods, the signal analysis is performed by a human using an off-chip device. This approach has the potential to lead to human error, is expensive, time consuming and unsuitable for portable lab-on-chip applications. With the growth of system-on-chip (SoC) technologies, it is possible to develop an on-chip analyser for nano-biosensors. Conventional signal analysis methods are perform using higher complexity algorithm to achieve higher accuracy on analysis results. However, higher complexity of algorithms will required higher power consumption for signal processing of the system. Therefore, conventional

Published manuscript link: http://dx.doi.org/10.1080/03091902.2016.1223195

methods are not suitable to apply into portable device, due to limited power supply on portable device. So, a new signal analysis algorithm is required for portable lab-on-chip applications.

2. NANO-BIO SENSOR REACTION

In this section, the latest nano-biosensor and amplitude response will be reviewed. The operation of the device will be discussed and the electrical signal output from the sensor will be highlighted. The authors in [1] proposed a novel polyurethane-heparin nanoparticle (PU-Hep NP) glucose biosensor, which is used to measure glucose levels in the blood directly. Figure 1 illustrates the SEM image of PU-Hep NPs. This device is an anti-interference device to uric acid and ascorbic acid which are present in the blood; hence, it can produce more accurate results compared to existing methods. The glucose concentration is determined by the current amplitude. Figure 2 illustrates the linear relationships between the peak current and the concentration of glucose in whole blood samples.

The authors in [2] proposed a laccase sensor to detect the concentration of a phenolic compound comprising caffeic acid, acid blue 74, azino-bis(3-ethyl benzo thiazoline-6 sulfonic acid) (ABTS) and ferulic acid. This sensor is used in such industries as fruits and beverages, paper, textiles and cosmetics. Figs. 3 and 4 show the results measurement of acid blue 74 and caffeic acid, respectively. The results show that there is a linear relation between the current amplitude and the substrates concentration.

The authors in [3] proposed using embryonic stem cells as cell-based biosensors for drugs screenings. This sensors record the change in beat frequency, duration and amplitude of cardiomyocytes, which is a muscle tissue of the heart. By monitoring this change, the drug-type taken by the patient can be determined. Figure 5 illustrates the extracellular potentials of the cardiomyocytes. The amplitude of the whole signal is used to analyse the sum amplitude of stroke one and stroke two. Figure 6 illustrates the amplitude response of cardiomyocytes to CARB, ISO and a physiological solution as a control with a 1 μM drug concentration.

The authors in [4] proposed a cardiomyocyte-based impedance sensor to detect the concentration of marin toxins in the human body, such as the saxitoxin (STX) and tetrodotoxin (TTX). The concentration is determined by analysing the recorded amplitude, cell index and beating rate from the sensor. Figure 7 illustrates the construction of the cardiomyocyte-based sensor. The sensor is built from a 96-well plate and integrated with a gold microelectrode in the bottom of each well. Figure 8 shows the output from this sensor. The beating signal is based on the rhythmic changes in cell attachment and morphology due to the contraction and relaxation of cardiomyocytes, which modulates the impedance signal accordingly.

The authors in [5] proposed an electrochemical impedance biosensor for the detection of biomolecules to measure the concentration of DNA. Figure 9 illustrates the idealization of the electrode-electrolyte interface. This sensor provides a capacitance readout with a small sample volume. The concentration of the DNA is detected by the capacitance change of the sensors. Figure 10

Published manuscript link: http://dx.doi.org/10.1080/03091902.2016.1223195

illustrates the results of the measurement. The results show that the $c_{cDNA}/_{Cd\text{-}change}$ as a function of c_{cDNA} in a log–log scale provide a very good linear relationship.

3. SIGNAL ANALYSIS

Section 2 discussed how nano-biosensors produce amplitude changes to identify or quantify the measured response. In order to interpret this result automatically, a proper signal analysis algorithm must be implemented. In this section, several methods for analysing the amplitude sensor signal will be discussed.

The authors in [6] proposed the R-peak detection of the ECG signal based on the peak of a Shannon energy envelop (SEE). This method is used for monitoring and analysing a real-time electrocardiogram (ECG). Figure 11 illustrates the block diagram of a peak of an SEE system. This method consists of three stages, which are a data preparation stage, SEE extraction and peak-finding. In the data preparation stage, the raw ECG signal is processed using a band-pass filter (BPF), differentiation (Diff) and amplitude transformation (AT). In the SEE extraction stage, the signal from the preparation stage will pass to Shannon transformation and low-pass filtering (LPF). The objective of this stage is to enclose the signal using a SEE. Next, the output will be passed to a peak-finding stage. In the peak-finding stage, the signal will be processed using peak detection, false-R detection (FRD) and false-noise detection (FND). The peak detected on the SEE is the peak of the signal. Figure 12 shows the peak detection for a real-time ECG signal. The total accuracy of this system can achieve above 99.83%.

The authors in [7] proposed an adaptive threshold method (ATM) for the peak detection of photoplethysmography (PPG)-based temporal analyses. This method is used for physiological and cardiovascular diagnosis, including blood volume change. This method consists of two parts, namely adaptive threshold detection and peak correction. Figure 13 illustrates this method. In the adaptive threshold detection part, the virtual threshold is increased or decreased with a fixed-slope parameter to detect the foot and the peak. This step is repeated with various slopes until every peak is found. Figure 13(a) illustrates that the solid line is a band-pass filtered PPG waveform, and the dashed line is a detection threshold. Vmax and Vmin are represented with '▼' and '▲', respectively. In the sensing period, the detection threshold is accompanied with the PPG waveform amplitude, while in the out-of-sensing period it is varied by a pre-defined slope parameter. At upper and lower inflections, the detection threshold reports the peak, and it is only valid when the peak is detected out of the refractory period. In the peak correction part, the algorithm is varied with the relation to the incident wave and the reflected wave to reduce the reflected wave amplitude. Figure 13(b) illustrates whether the detected peak is found in the refractory period, while the detected peak is ignored(∇) and the threshold level is not affected by the ignored peak. This method has been applied to a PPG waveform and it achieves 98.22% accuracy.

Published manuscript link: http://dx.doi.org/10.1080/03091902.2016.1223195

The authors in [8] proposed an automatic chromatographic peak detection (ACPD) method. This method is used to analyse the chromatographic fingerprints of complex samples, including botanical extracts and urine samples. Figure 14 illustrates the framework of ACPD. This method consists of five stages, which are preliminary chromatographic peak detection, automatic instrumental noise-level estimation, pseudo-peak elimination, chromatographic peak clustering and peak baseline estimation, and small peak elimination. Figure 15 illustrates the ACPD signal processing stages. First, the signal will be processed by the preliminary chromatographic peak-detection stage. At this stage, each peak's start position and end position is identified. Afterwards, the signal is processed in the automatic instrumental noise-level estimation stage. At this stage, the instrumental noise-level and threshold value for the first-order derivative is calculated. The example results are shown in Figure 15 (C). Next, the false peak is eliminated in the pseudo-peak elimination stage based on the threshold value. Next, in the chromatographic peak clustering and peak baseline estimation stage is calculated the average signal-to-noise ratio (ASNR). At the end, the peak with an ASNR smaller than the instrumental noise level is eliminated in the small-peak elimination stage.

The authors in [9], [10] proposed the auto-threshold peak-detection method for a portable multi-model nano-biosensor system and for physiological signal detection. This method consists of two stages, namely cluster-mean calculation and peak detection. In the cluster-mean calculation stage, the sample is assigned to the nearest cluster-mean, and the new cluster-mean is determined after all of the sample is assigned. This step is repeated until the cluster-mean is less than the termination condition. In the peak-detection stage, the larger cluster-mean is used as the threshold value. A peak is defined when the local maxima is between a leading edge and a falling edge, whereby the edge is larger than the threshold value. Figure 16 illustrates the peak detection for the final output of the noise signal using the auto-threshold algorithm.

The authors in [11] proposed an automatic multi-scale-based peak-detection (AMPD) method for automatic peak detection in noisy periodic and quasi-periodic signals. This method is applicable to many real-world signals, including the blood-volume pulse in functional near-infrared spectroscopy (fNIRS) signals and the maximum concentration of expired CO_2, QRS peak in ECG signals. Figure 17 illustrates the calculation steps of the AMPD algorithm. This method consists of four steps, namely a local maxima scalogram (LMS) calculation, the row-wise summation of the LMS, LMS rescaling and peak detection. Figure 18 presents an example of applying the AMPD algorithm to a simulated signal. First, the LMS is calculated. In this step, the local maxima is determined using a moving-window approach and a matrix is formed based on the LMS of the signal. Figure 18(a) illustrates the local maxima scalogram. Next, the LMS rescaling step is performed to reshape the LMS matrix to the row of lowest row-wise summation. Figure 18(b) illustrates the rescaled LMS. Afterwards, the row-wise summation of the LMS is performed whereby, in this step, the algorithm performs a row-wise summation of the LMS matrix. Figure 18(c) illustrates the row-wise summation of every row. In the last step, the peaks are determined by calculating the column-wise standard deviation of the matrix after it is

Published manuscript link: http://dx.doi.org/10.1080/03091902.2016.1223195

reshaped. Figure 18(d) shows the calculated row-wise standard deviation of the rescaled LMS. Figure 18(e) and (f) shows the detected peaks.

Table 1 summarizes the algorithm discussed in Section 3. From the table, the amplitude signal analysis can be divided into three stages. They are: signal pre-processing, peak detection and signal correction. At the signal pre-processing stage, the main purpose is to remove the noise of the signal. In [6], [8] and [11], methods such as a band-pass filter, differentiation, amplitude transformation, noise level, peak clustering, baseline estimation and window moving are used in the pre-processing stage. This stage is important to avoid any false signal due to noise.

Once the signal has been processed, the next stage is signal analysis, which is the main step of the analysis. The methods used in this stage include SEE extraction, virtual threshold, local maxima, threshold calculation and a local maxima scalogram. The SEE is able to detect the R-peak of the ECG signal with 99.83% accuracy.

In the final step, signal correction is performed. This step sees the removal of the noise peak or any wrongly detected peak to increase the accuracy of the final result. Papers [6], [7] and [8] incorporate this step in their algorithm. The methods used include FRD, FND, refractory period and peak elimination. FRD, FND and refractory period utilize a time interval as the reference to eliminate the wrong peak. This step can eliminate most of the peak noise for a periodic signal. Peak elimination in ACPD eliminates the peak located outside the range between of high-positive and high-negative gradient of the signal. This method is able to eliminate most of the noise peak.

4. DISCUSSIONS

As discussed in Section 2, different nano-biosensors react differently to produce the amplitude changes to its output current or voltage. Some sensors produce a periodic signal with different amplitudes, while others produce amplitude changes to a non-periodic output signal. To process this signal, we have to look at several algorithms that are subjected to various signal amplitude analyses, as discussed in Section 3. While the methods in Section 3 are not specifically designed for a nano-biosensor, these methods can still be used to analyse a nano-biosensor signal since the signals have similar characteristics.

To optimize the signal analysis algorithms, there are two main criteria have to be concern, which are complexity and performance accuracy. Base on the review in Section 3, ATPD has lowest complexity among the reviewed methods since it only consist of two processes. Therefore, ATPD will be proposed for portable lab-on-chip applications. However, to achieve the requirement of portable lab-on-chip applications, reduce the complexity is required. Hence, an modified version of threshold calculation method is suggested in order to reduce the complexity. To achieve the requirement for biomedical application, a high accuracy device is needed. Therefore, improvement in peak detection method is recommended. Current ATPD is able to perform

Published manuscript link: http://dx.doi.org/10.1080/03091902.2016.1223195

peak detection on biosignal and physiological signal. Hence, a specified peak detection on a nanoscale biosensor analysis method is proposed, so that improvement of accuracy can be achieve in a specific application without increase the complexity.

5. CONCLUSIONS

In this paper, the latest existing nano-biosensors with an amplitude response have been reviewed. Each sensor produces a different output signal depending upon their electrical characteristics. In addition, several peak-detection algorithms have also been reviewed. Based on our analysis, the amplitude peak detection requires three main steps, which are signal pre-processing, signal analysis and signal correction. Furthermore, specific algorithms work well in certain types of signal, such as periodic or non-periodic signals. Base on the reviewed methods, the criteria in development of a signal processing algorithm for nanoscale biosensor in portable device application are low complexity and high accuracy detection. To evaluate the performance of each algorithm, the next phase of our work will benchmark each algorithm's performance with respect to its peak detection accuracy.

6. ACKNOWLEDGEMENTS

This research was supported by the Fundamental Research Grant Scheme, Ministry of Higher Education, Malaysia (FRGS Phase 1, 2014).

REFERENCES

[1] C. Sun, Y. Niu, F. Tong, C. Mao, X. Huang, B. Zhao, and J. Shen, "Preparation of novel electrochemical glucose biosensors for whole blood based on antibiofouling polyurethane-heparin nanoparticles," *Electrochim. Acta*, vol. 97, May 2013, pp. 349–356.

[2] H. García-Arellano, D. Fink, G. Muñoz Hernández, J. Vacík, V. Hnatowicz, and L. Alfonta, "Nuclear track-based biosensors with the enzyme laccase," *Appl. Surf. Sci.*, vol. 310, Aug. 2014, pp. 66–76.

[3] Q. Liu, H. Huang, H. Cai, Y. Xu, Y. Li, R. Li, and P. Wang, "Embryonic stem cells as a novel cell source of cell-based biosensors.," *Biosens. Bioelectron.*, vol. 22, no. 6, Jan. 2007, pp. 810–5.

[4] Q. Wang, K. Su, L. Hu, L. Zou, T. Wang, L. Zhuang, N. Hu, and P. Wang, "A novel and functional assay for pharmacological effects of marine toxins, saxitoxin and tetrodotoxin by cardiomyocyte-based impedance biosensor," *Sensors Actuators B Chem.*, vol. 209, Mar. 2015, pp. 828–837.

[5] L. Ianeselli, G. Grenci, C. Callegari, M. Tormen, and L. Casalis, "Development of stable and reproducible biosensors based on electrochemical impedance spectroscopy: three-electrode versus two-electrode setup.," *Biosens. Bioelectron.*, vol. 55, May 2014, pp. 1–6.

[6] H. Zhu and J. Dong, "An R-peak detection method based on peaks of Shannon energy envelope," *Biomed. Signal Process. Control*, vol. 8, no. 5, Sep. 2013, pp. 466–474.

Published manuscript link: http://dx.doi.org/10.1080/03091902.2016.1223195

[7] H. S. Shin, C. Lee, and M. Lee, "Adaptive threshold method for the peak detection of photoplethysmographic waveform.," *Comput. Biol. Med.*, vol. 39, no. 12, Dec. 2009, pp. 1145–52.

[8] Y.-J. Yu, Q.-L. Xia, S. Wang, B. Wang, F.-W. Xie, X.-B. Zhang, Y.-M. Ma, and H.-L. Wu, "Chemometric strategy for automatic chromatographic peak detection and background drift correction in chromatographic data.," *J. Chromatogr. A*, vol. 1359, Sep. 2014, pp. 262–70.

[9] J. Park, J. Song, H. Kim, and D. Ryu, "Peak Detection for Portable Multi-modal Nano-bio Sensor System," *Int. J. Bio-Science Bio-Technology*, vol. 5, no. 3, 2013, pp. 135–142.

[10] a. L. Jacobson, "Auto-threshold peak detection in physiological signals," *2001 Conf. Proc. 23rd Annu. Int. Conf. IEEE Eng. Med. Biol. Soc.*, vol. 3, 2001, pp. 2194–2195.

[11] F. Scholkmann, J. Boss, and M. Wolf, "An Efficient Algorithm for Automatic Peak Detection in Noisy Periodic and Quasi-Periodic Signals," *Algorithms*, vol. 5, no. 4, Nov. 2012, pp. 588–603.

Published manuscript link: http://dx.doi.org/10.1080/03091902.2016.1223195

Table 1. Comparison of amplitude algorithms

Algorithms	[6]	[7]	[8]	[9,10]	[11]
Abbreviation	PSEE	ATM	ACPD	ATPD	AMPD
Type of signal	Periodic	Periodic	Non	Non	Periodic or quasi-periodic
Signal source	ECG	PPG	Chromato-graphic	Biosensor signal and ECG	Any real-time signal
Signal Pre-processing	BPF, Diff, AT	NA	Noise level, peak clustering and base line estimation	NA	Window moving
Signal analysis	SEE extraction	Virtual threshold	Local maxima	Threshold calculation	LMS
Signal Correction	FRD, FND	Refractory period	Peak eliminations	NA	NA
Complexity	High	Low	High	Low	High

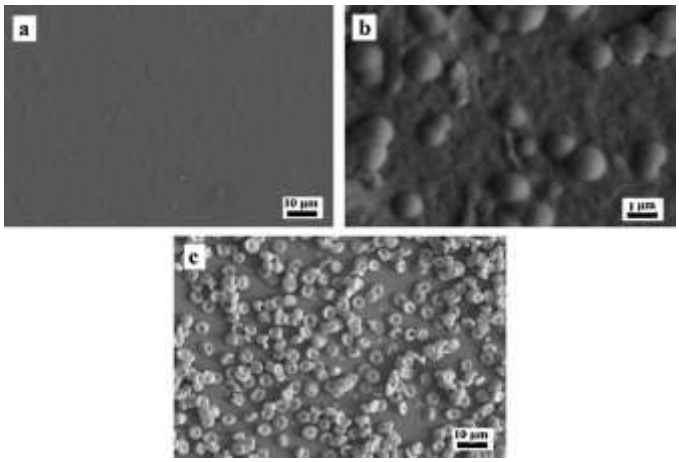

Figure 1. SEM images of (a) an electrode substrate modified with GOx/(PU-Hep), (b) enlarged view from (a), and (c) blank electrode substrate exposed to human whole blood samples for 60 min, respectively [1].

Published manuscript link: http://dx.doi.org/10.1080/03091902.2016.1223195

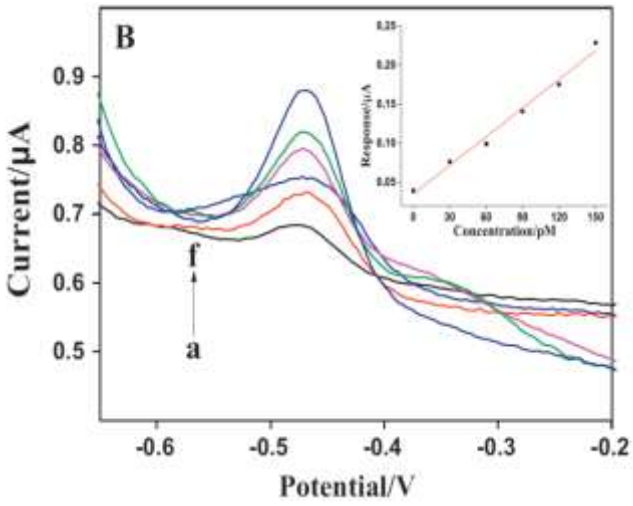

Figure 2. Differential pulse voltammetry (DPV) obtained for glucose oxidase (GOx) modified (PU-Hep)/glass carbon electrode (GCE) in whole blood samples at 25◦C with various levels of glucose. The insert: relationship between the peak current and the concentration of glucose in whole blood samples [1].

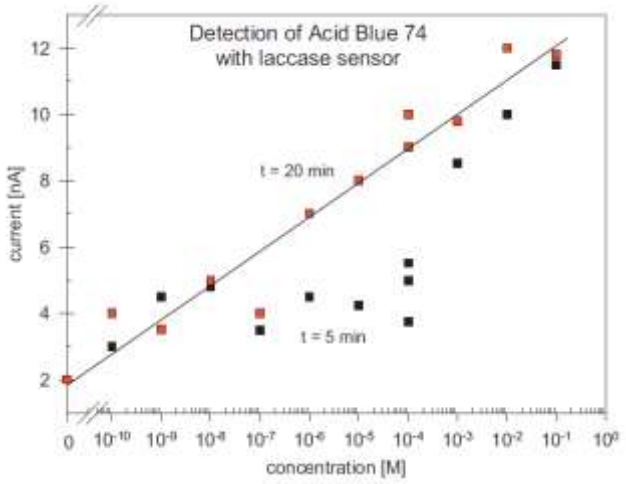

Figure 3. Calibration curve for acid blue 74 determination; sensor with conical-type etched tracks [2].

Published manuscript link: http://dx.doi.org/10.1080/03091902.2016.1223195

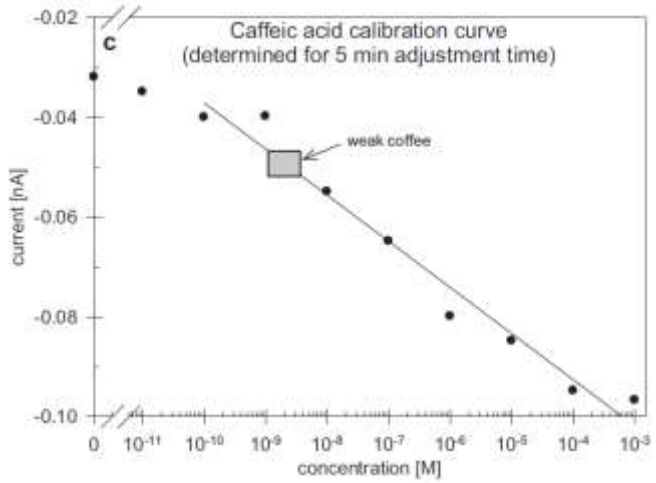

Figure 4. Sensing of caffeic acid by a laccase-clad track-based biosensor with a conical- type geometry [2].

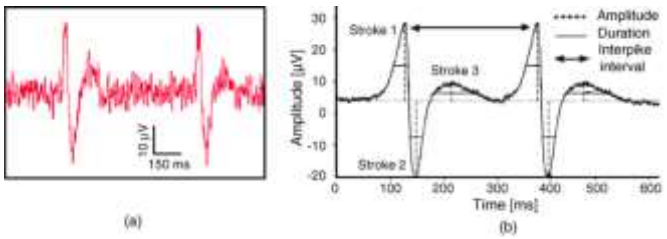

Figure 5. Extracellular potentials of the cardiomyocytes, with the drug-screening parameters of the signals indicated [3].

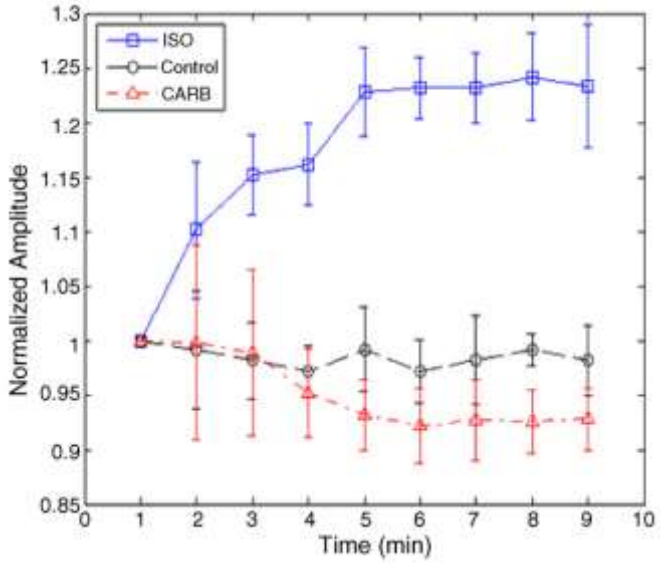

Figure 6. Plots comparing the amplitude response of cardiomyocytes to the carbamylcholine (CARB), isoproterenol (ISO) and a physiological solution as a control [3].

Published manuscript link: http://dx.doi.org/10.1080/03091902.2016.1223195

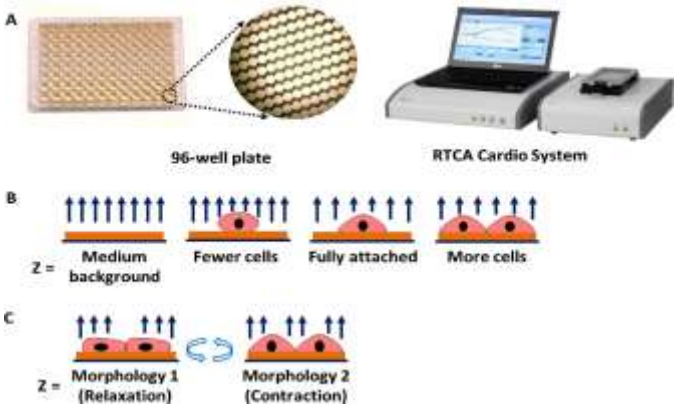

Figure 7. Construction of the cardiomyocyte-based biosensor [4].

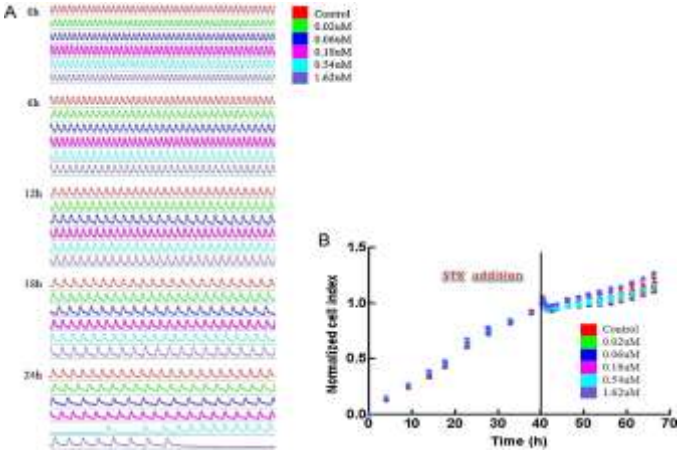

Figure 8. Dynamic monitoring of the attachment, growth and beating activity of rat cardiomyocytes in the presence of STX. (A) Snapshots of representative beating profiles at selected time points after exposure to STX of increasing concentrations at 24 h. Each snapshot spanned for a duration of 20 s. (B) Normalized cell index of cardiomyocytes before and after STX treatment [4].

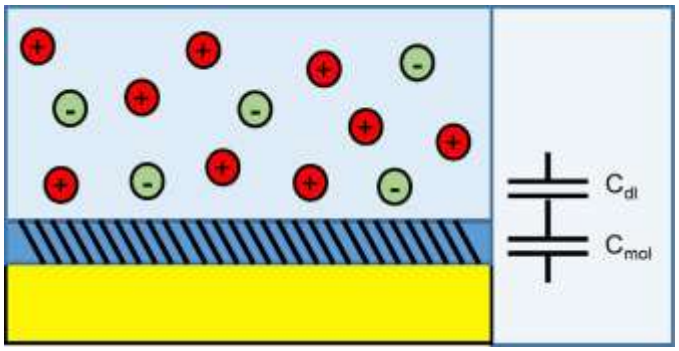

Figure 9. Idealization of the electrode-electrolyte interface [5].

Published manuscript link: http://dx.doi.org/10.1080/03091902.2016.1223195

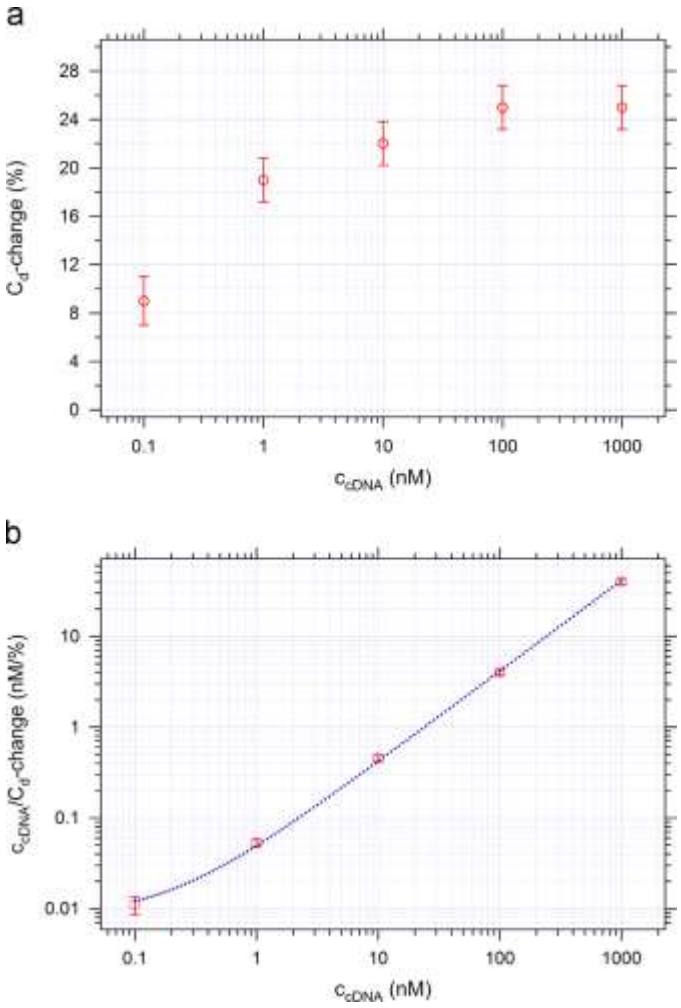

Figure 10. Calibration curve of the three-electrode device [5].

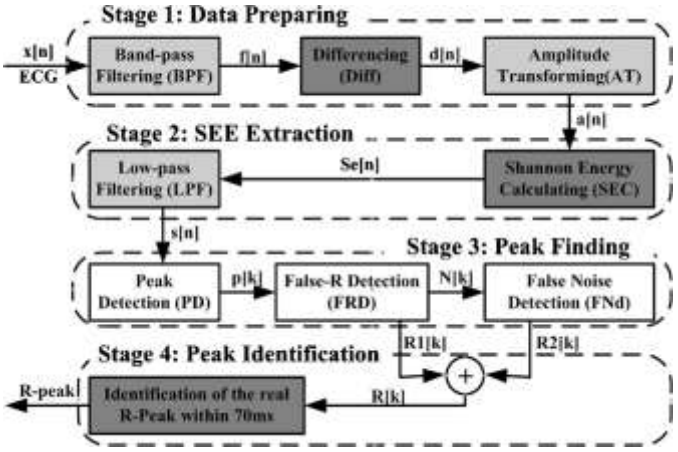

Figure 11. Block diagram of the peak of the SEE. The deep grey, shallow grey and white backgrounds indicate original, improved and newly introduced parts, respectively [6].

Published manuscript link: http://dx.doi.org/10.1080/03091902.2016.1223195

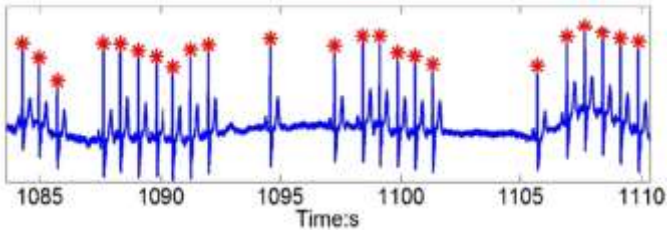

Figure 12. Peak detection of the ECG signal [6].

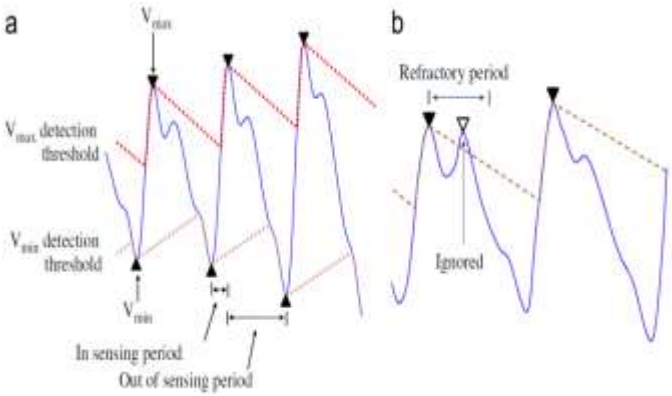

Figure 13. Adaptive threshold detection method [7].

Published manuscript link: http://dx.doi.org/10.1080/03091902.2016.1223195

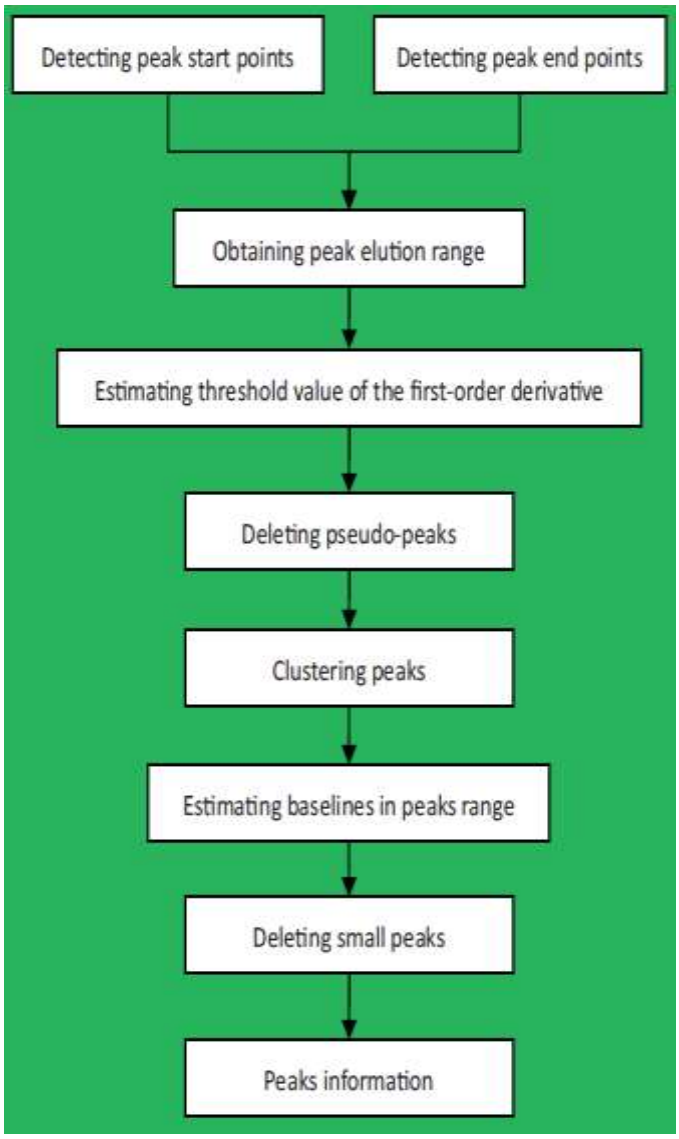

Figure 14. Flow diagram showing the framework of ACPD [8].

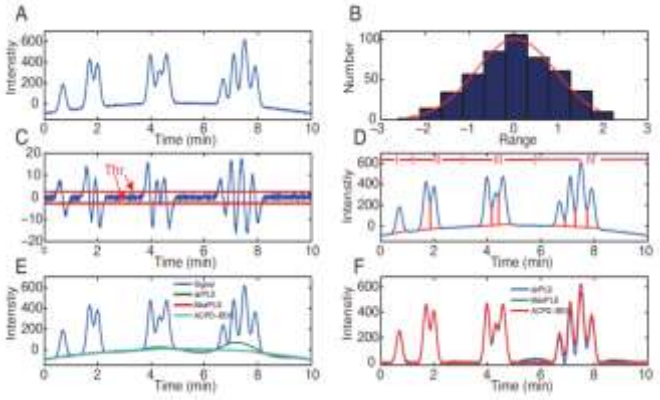

Figure 15. The ACPD signal processing stage [8].

Published manuscript link: http://dx.doi.org/10.1080/03091902.2016.1223195

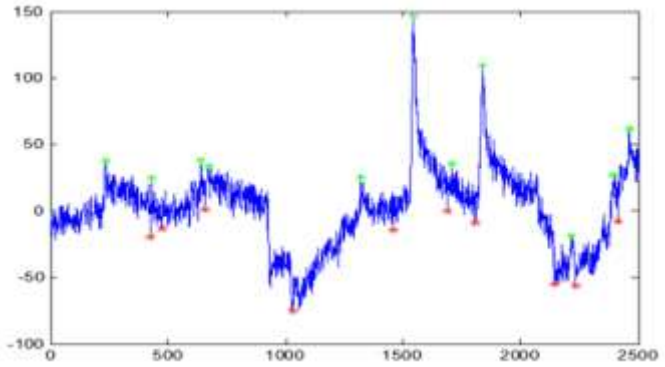

Figure 16. Peak detection results of the auto-threshold algorithm [9].

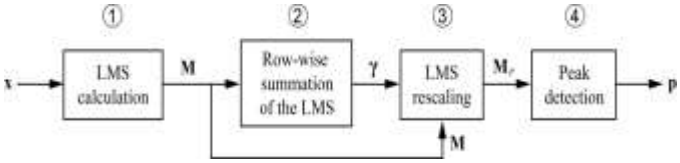

Figure 17. Calculation steps of the AMPD algorithm [11].

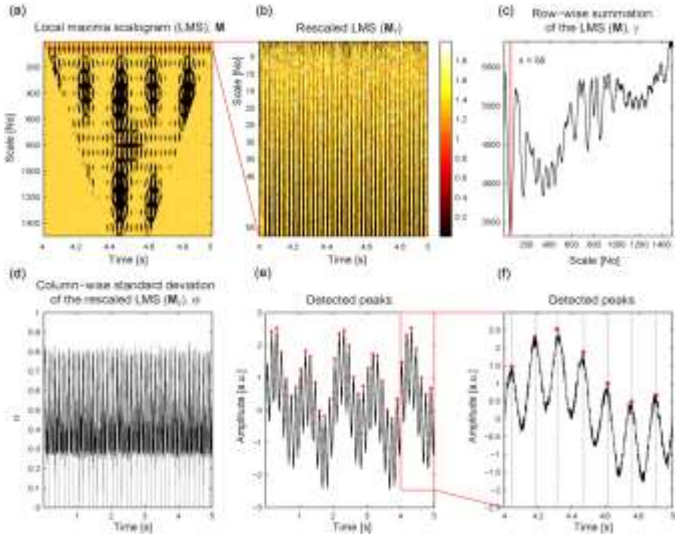

Figure 18. Example showing the application of the AMPD algorithm to a simulated signal [11].

Published manuscript link: http://dx.doi.org/10.1080/03091902.2016.1223195